Diamond & Related Materials 66 (2016) 119–125

Contents lists available at ScienceDirect

Diamond & Related Materials

journal homepage: www.elsevier.com/locate/diamond

Synthesis of microporous carbon/graphene composites for high-performance supercapacitors

Xiaojun He [a,*], Jingxian Wang [a], Guohui Xu [a], Moxin Yu [a], Mingbo Wu [b,*]

[a] School of Chemistry and Chemical Engineering, Anhui Key Lab of Coal Clean Conversion and Utilization, Anhui University of Technology, No. 59 Hudong Road, Maanshan 243002, China
[b] State Key Lab of Heavy Oil Processing, China University of Petroleum, Qingdao 266580, China

ARTICLE INFO

Article history:
Received 15 November 2015
Received in revised form 5 April 2016
Accepted 5 April 2016
Available online 14 April 2016

Keywords:
Coal tar pitch
Graphene
Composite
High capacitance
Supercapacitor

ABSTRACT

Microporous carbon/graphene composites (MPC/Gs) are prepared for the first time directly from coal tar pitch and graphene oxide by KOH activation. MPC/Gs are characterized by scanning electron microscopy, transmission electron microscopy, X-ray diffraction, and nitrogen adsorption-desorption techniques. The electrochemical properties of MPC/G composites are examined by cyclic voltammetry, galvanostatic charge-discharge and electrochemical impedance spectroscopy. MPC/$G_{10\text{-}2\text{-}24}$ made with the mass ratio of coal tar pitch, graphene oxide and KOH at 10/2/24 possesses both high surface area and good electrochemical performance. When evaluated as electrodes of supercapacitors, MPC/$G_{10\text{-}2\text{-}24}$ exhibits high specific capacitance (278 F g^{-1} at 0.05 A g^{-1}), good rate performance (218 F g^{-1} at 20 A g^{-1}) and excellent cycle stability (93% capacitance retention after 10,000 cycles). This work paves a facile method to produce composite materials, which is believed to be of interest for a wide audience of readers in the fields of energy conversion and storage.

© 2016 Elsevier B.V. All rights reserved.

1. Introduction

In recent years, the development of new energy vehicles are sharply promoted by energy crisis, and thus accelerate the development of the energy storage devices such as fuel cells, lithium-ion batteries, and supercapacitors [1]. Supercapacitor, also known as electrochemical capacitor [2], is a capacitor which stores charges via either ion adsorption at the interface of electrode and electrolyte or fast surface redox reaction. Recently, supercapacitor has received great attention because of its long cycle life and high power density [3–7], and being used to complement or partially replace batteries in various energy storage applications [8]. The electrode materials are known as the key components determining their capacitance performance, and porous carbons are the most reported electrode materials for supercapacitors owing to their high surface area, good chemical stability and low cost [9–12]. Unfortunately, conventional porous carbon, especially microporous carbon suffers from poor rate performance at high rate, which limits its wide applications. Graphene, a two-dimensional (2D) monolayer of sp^2-hybridized carbon atoms, has attracted enormous attention for various applications, owing to its distinctive chemical and physical properties [13–15]. Compared with traditional porous carbon materials, graphene features with high electrical conductivity [16]. Yet, the restacking and aggregation during electrode manufacturing is easy to occur in graphene, which results in the decreases both in surface area available and the supercapacitive performance. Various carbon-based materials have been discovered and investigated intensively as the electrode materials to improve the electrochemical performance of supercapacitors [17–21]. The diversity of structures and bonding schemes of carbon materials provide versatility in properties and applications. There is no doubt that composite of different carbon materials would extend the diversity of carbon-based materials, featuring with integrated properties inherited from the constituent structures. Compared to the single component, composite materials such as graphene/carbon nanotubes [4,17], graphene/activated carbon [19] and carbon nanotubes/activated carbon [22], have shown improved electric or thermal properties, due to the synergistic effects from different carbon components. However, the single component in the composite is usually synthesized separately, followed by being mixed [22], i.e. the single component in the composite are mainly connected via physical contact, which not only increase the production cost of composite materials but also reduce the performance of the composite materials.

Herein, a facile method is reported for the first time for the synthesis of microporous carbon/graphene composites (MPC/Gs) directly from coal tar pitch (CTP) and graphene oxide (GO) by KOH activation to realize the bonding of the two components in the composite. GO is coated with microporous carbon derived from the liquefied and activated CTP uniformly, which not only prevent the restacking of GO but also improve the utilization of GO and the stability of the composite. The aim of this work is to introduce a facile method for the production of low-cost composite electrode materials for high-performance supercapacitors.

* Corresponding authors.
E-mail addresses: agdxjhe@126.com (X. He), wumb@upc.edu.cn (M. Wu).

http://dx.doi.org/10.1016/j.diamond.2016.04.005
0925-9635/© 2016 Elsevier B.V. All rights reserved.

2. Experimental

2.1. Synthesis of MPC/G composite

GO used here was prepared from natural graphite by the modified Hummers method as described elsewhere [23,24]. The synthesis of MPC/G composite was performed by KOH activation as follows. Firstly, 1 g of GO powder was added into 200 mL of *N*,*N*-dimethyl formamide (DMF) and dispersed under ultra-sonication for 60 min. Secondly, 5 g CTP was added into the homogeneous GO suspension (5 mg mL^{-1}) and sonicated for 60 min. After that, the solid carbon precursor was obtained by stirring using magnetic stirrer, followed by drying the pasty solid at 383 K for 12 h. Subsequently, the carbon precursor was mixed with 12 g KOH in solid state and heated in a tube furnace at a heating rate of 5 K min^{-1} to 1073 K and kept for 1 h by electric heating under nitrogen atmosphere (99.999%, 60 mL min^{-1}). After cooling down to room temperature, the resultant sample was washed by 2 M HCl solution and distilled water thoroughly to remove the ions. The as-made MPC/G composite is termed as MPC/$G_{x\text{-}y\text{-}z}$, where the subscript x-y-z refers to the mass ratio of CTP, GO and KOH. For comparison, GO was activated by using KOH as activation agent in a tube furnace at a heating rate of 5 K min^{-1} to 873 K and kept for 1 h by electric heating under nitrogen atmosphere, of which the low temperature is used to activate GO in order to get high carbon yield. Before test and characterization, the as-made MPC/G composite was ground to a fine powder with a particle size below 44 μm.

2.2. Characterization of MPC/G composite

The pore structure of the as-made MPC/G composite was analyzed by nitrogen adsorption-desorption isotherms at 77 K (ASAP2010). The BET surface area (S_{BET}) of MPC/G composite was calculated by the BET (Brunauer-Emmett-Teller) equation. The pore size distribution of MPC/G composite was calculated by the density functional theory (DFT) method. The total pore volume (V_t) was obtained at a relative pressure of 0.99. The micropore volume (V_{mic}) of MPC/G composite was estimated by using the t-plot method. The mesopore volume (V_{meso}) was calculated from the difference of V_t and V_{mic}. The average pore size (D_{ap}) of MPC/G composite was obtained by the equation of $D_{ap} = 4V_t/S_{BET}$. The morphology and microstructure of MPC/G composite were investigated by using filed emission scanning electron microscopy (FESEM, Nanosem 430) with energy dispersive spectrum (EDS), transmission electron microscopy (TEM, JEOL-2100), and X-ray diffraction (XRD, Philips X, pert Prosuper, Cu Kα, Radiation). The chemical bonding states of carbon, oxygen and nitrogen elements in MPC/G composite were analyzed by X-ray photoelectron spectroscopy (XPS, Thermo ESCALAB250, USA). The Raman spectra of MPC/G composite were recorded on a Raman spectroscopy (JYLab-Ram HR800, excited by a 532 nm laser).

2.3. Preparation and electrochemical test of MPC/G composite electrodes

The electrode slurry was fabricated by mixing MPC/G composite, carbon black with a BET surface area of 550 m^2 g^{-1} and poly(tetrafluoroethylene) at a mass ratio of 83:12:5 in ethanol until slurry formed. The resultant slurry was rolled into thin film (ca. 5 μm in thickness) and dried at 383 K for 2 h under vacuum before being coated onto the nickel foam at 15 MPa for 10 s. Before the electrochemical test, the electrodes was soaked overnight in 6 M KOH aqueous electrolyte, 1 M Et_4NBF_4 organic electrolyte, 1-butyl-3-methylimidazolium hexafluorophosphate ($BMIMPF_6$) ionic liquid electrolyte, respectively [25]. Button-type supercapacitor was assembled with two similar carbon electrodes (4 mg cm^{-2}) separated by polypropylene membrane.

The supercapacitor was evaluated by cyclic voltammetry (CV) and electrochemical impedance spectroscopy (EIS) on an electrochemical workstation (CH Instrument, Shanghai, China). The gravimetric capacitance of MPC/G composite electrodes (C, F g^{-1}) was calculated from the CV curves according to Eq. (1).

$$C = \frac{2\int_{V_1}^{V_2} i(V)dV}{mv\Delta V} \tag{1}$$

where V_1 and V_2 (V) are the lower and upper limits of potential in a cyclic potential sweep, respectively; $\Delta V = V_2 - V_1$, is the voltage window; v is the scan rate (V s^{-1}); $i(V)$ is the current as the function of voltage, and m is the mass (g) of active material in single electrode.

The galvanostatic charge/discharge was determined on the supercapacitance test system (SCTs, Arbin Instruments, USA). The cut off charge voltage for the supercapacitor in 6 M KOH aqueous was set at −0.9 ~ 0.1 V. The gravimetric capacitance of the MPC/G composite electrode (C, F g^{-1}) was also calculated from the discharge curve according to Eq. (2).

$$C = \frac{2I\Delta t}{m \times \Delta V} \tag{2}$$

where I is the discharge current (A), ΔV is the discharge voltage between the Δt period, and m is the mass (g) of the active materials in single electrode.

The electrochemical impedance spectroscopy (EIS) measurements were performed with amplitude of 5 mV over the frequency range from 100 kHz to 0.001 Hz using an electrochemical workstation (CH Instrument, Shanghai, China). The gravimetric capacitance of MPC/G composite electrodes (C, F g^{-1}) was also obtained according to Eq. (3).

$$C = -\frac{4}{2\pi mfZ_{Im}} \tag{3}$$

where f is the frequency (Hz), m is the mass (g) of the active material in single electrode, and Z_{Im} is the imaginary impedance.

The energy density (E, W h kg^{-1}) and average power density (P, W kg^{-1}) of supercapacitors were calculated according to Eqs. (4) and (5).

$$E = \frac{1}{2 \times 4 \times 3.6} CV^2 \tag{4}$$

$$P = \frac{E}{\Delta_{td}} \tag{5}$$

where C is the capacitance of the two-electrode supercapacitor (F), and V is the usable voltage after the IR drop (V), and Δ_{td} is the time (h) for the discharge.

3. Results and discussion

3.1. The structure of MPC/G composite

Fig. 1a is the FESEM image of GO, showing the thick sheets in GO. After being activated by KOH at 873 K for 1 h, the as-made activated graphene (MPC/$G_{0\text{-}12\text{-}24}$) in Fig. 1b shows very thin sheet-like structure. Yet, the yield of MPC/$G_{0\text{-}12\text{-}24}$ is only 27.1%, indicating it is an uneconomic production process for the direct activation of GO because of the high cost of GO. As shown in Fig. 1c, MPC/$G_{12\text{-}0\text{-}24}$ features solid particles with many smooth walls. With the addition of GO, the morphology of MPC/G composite was transformed into big interconnected porous solid particles (Fig. 1d and e), which might be ascribed to the connection function of GO. Fig. 1f shows that thin graphene sheets are incorporated into MPCs. The graphene sheets in Fig. 1f are bonded in the MPC/G composites, which not only prevent the restacking of single graphene sheet and improve the utilization of expensive graphene, but also decrease the production cost of the composite materials. The closely combined

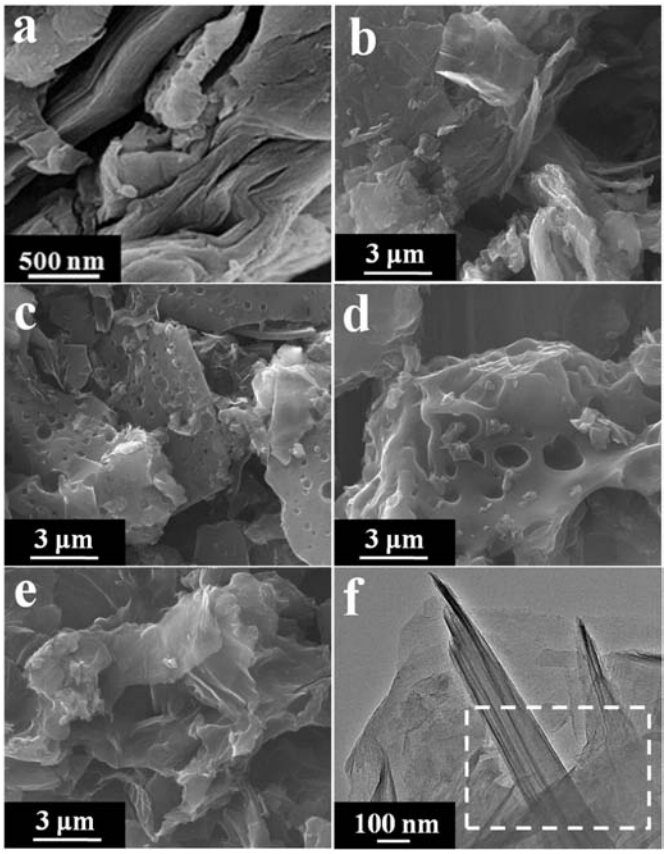

Fig. 1. FESEM images of: (a) GO; (b) MPC/$G_{0\text{-}12\text{-}24}$; (c) MPC/$G_{12\text{-}0\text{-}24}$; (d) MPC/$G_{10\text{-}2\text{-}24}$; (e) MPC/$G_{8\text{-}4\text{-}24}$; (f) TEM image of MPC/$G_{10\text{-}2\text{-}24}$.

graphene and microporous carbon is expected to increase the electron conduction and improve the supercapacitive performance. The pore structure characteristics of MPC/G composites were studied by nitrogen adsorption-desorption technique. The adsorption-desorption isotherms of the MPC/G composites are shown in Fig. 2a and b, respectively to show the difference between them clearly. The nitrogen adsorption-desorption isotherms of MPC/$G_{10\text{-}2\text{-}24}$ composite in Fig. 2a are typical IV type isotherms with strong N_2 adsorption at low pressure and a loop at relative pressure of 0.5–1.0, indicating the presence of micropore and some mesopore [1,3]. Fig. 2c is the pore size distribution of the MPC/G composites. The micropores and mesopores of MPC/$G_{10\text{-}2\text{-}24}$, MPC/$G_{9\text{-}3\text{-}24}$ and MPC/$G_{8\text{-}4\text{-}24}$ are in the range of 0.5–2.5 nm, which are wider than those of MPC/$G_{12\text{-}0\text{-}24}$. The pore structure parameters of the MPC/G composites are summarized in Table 1. The V_t of MPC/G composite rises from 0.83 $cm^3\ g^{-1}$ (MPC/$G_{11\text{-}1\text{-}24}$) to 1.11 $cm^3\ g^{-1}$ (MPC/$G_{10\text{-}2\text{-}24}$), then drops to 0.82 $cm^3\ g^{-1}$ (MPC/$G_{8\text{-}4\text{-}24}$) with the increase of GO mass from 1 to 4 g corresponding to the decrease of CTP mass from 11 to 8 g in the reactants with the other conditions remaining unchanged. The S_{BET} of MPC/$G_{10\text{-}2\text{-}24}$ and MPC/$G_{9\text{-}3\text{-}24}$ reaches 2164 and 2233 $m^2\ g^{-1}$, respectively, which is bigger than that of porous carbon reported in our previous work [25]. The V_t and S_{BET} of the MPC/G composite are higher than those of MPC/$G_{10\text{-}0\text{-}24}$ and MPC/$G_{0\text{-}12\text{-}24}$ made with the absence of CTP or GO, indicating the synergistic effect between CTP and GO used for the synthesis of composite. Besides, the yield of MPC/$G_{0\text{-}12\text{-}24}$ is 27.1%, which is only about 50% of that of MPC/G composite, meaning high synthesis efficiency of MPC/G composite from CTP and GO. The micropore percentage of MPC/$G_{11\text{-}1\text{-}24}$, MPC/$G_{10\text{-}2\text{-}24}$, MPC/$G_{9\text{-}3\text{-}24}$, MPC/$G_{8\text{-}4\text{-}24}$ ranges from 81.98% to 88.35%, belonging to microporous carbons [25]. The above results show that the pore structure parameters can be adjusted by changing the mass of carbon precursors in the reactants.

The crystal structure of the MPC/G composites was characterized by XRD and the results are depicted in Fig. 3a. The XRD pattern exhibits

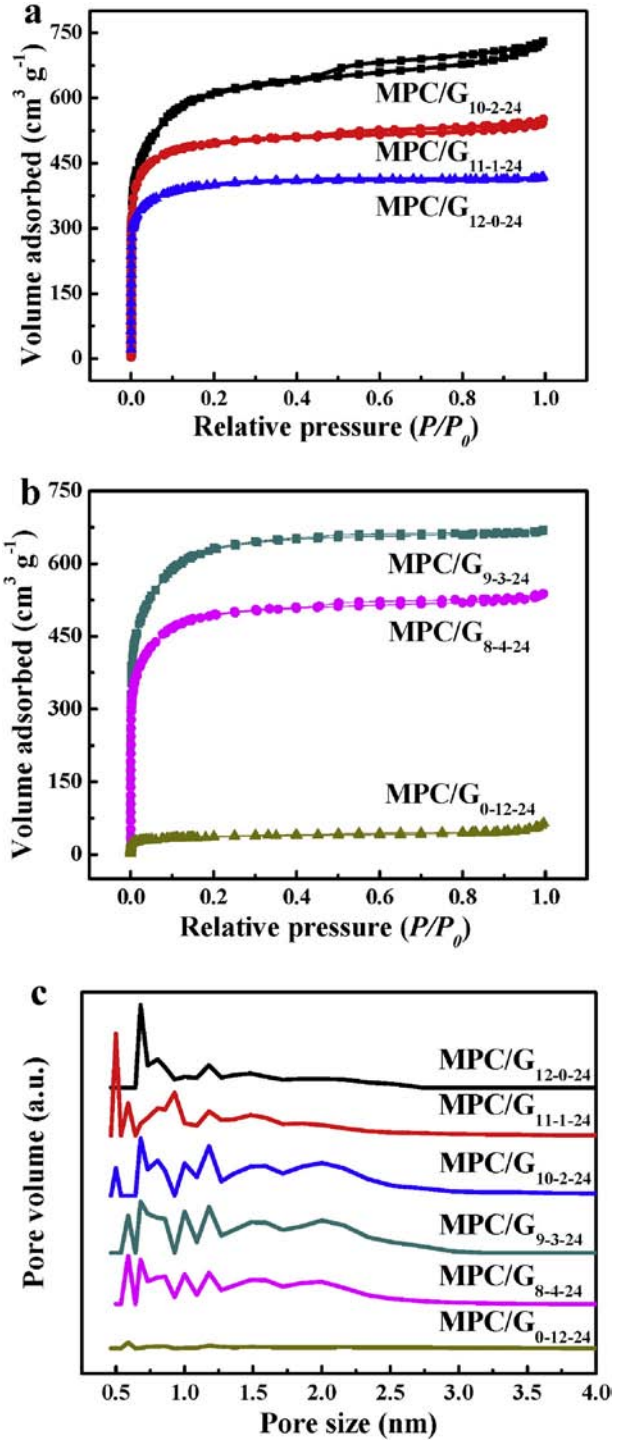

Fig. 2. (a, b) Nitrogen adsorption-desorption isotherms; (c) pore size distribution of MPC/G composites.

Table 1
The pore structure parameters of the MPC/G composites.

MPC/G samples	D_{ap} (nm)	S_{BET} ($m^2\ g^{-1}$)	V_t ($cm^3\ g^{-1}$)	V_{mic} ($cm^3\ g^{-1}$)
MPC/$G_{12\text{-}0\text{-}24}$	1.79	1436	0.64	0.61
MPC/$G_{11\text{-}1\text{-}24}$	1.87	1772	0.83	0.72
MPC/$G_{10\text{-}2\text{-}24}$	2.04	2164	1.11	0.91
MPC/$G_{9\text{-}3\text{-}24}$	1.85	2233	1.03	0.91
MPC/$G_{8\text{-}4\text{-}24}$	1.88	1749	0.82	0.72
MPC/$G_{0\text{-}12\text{-}24}$	2.66	130	0.09	0.05

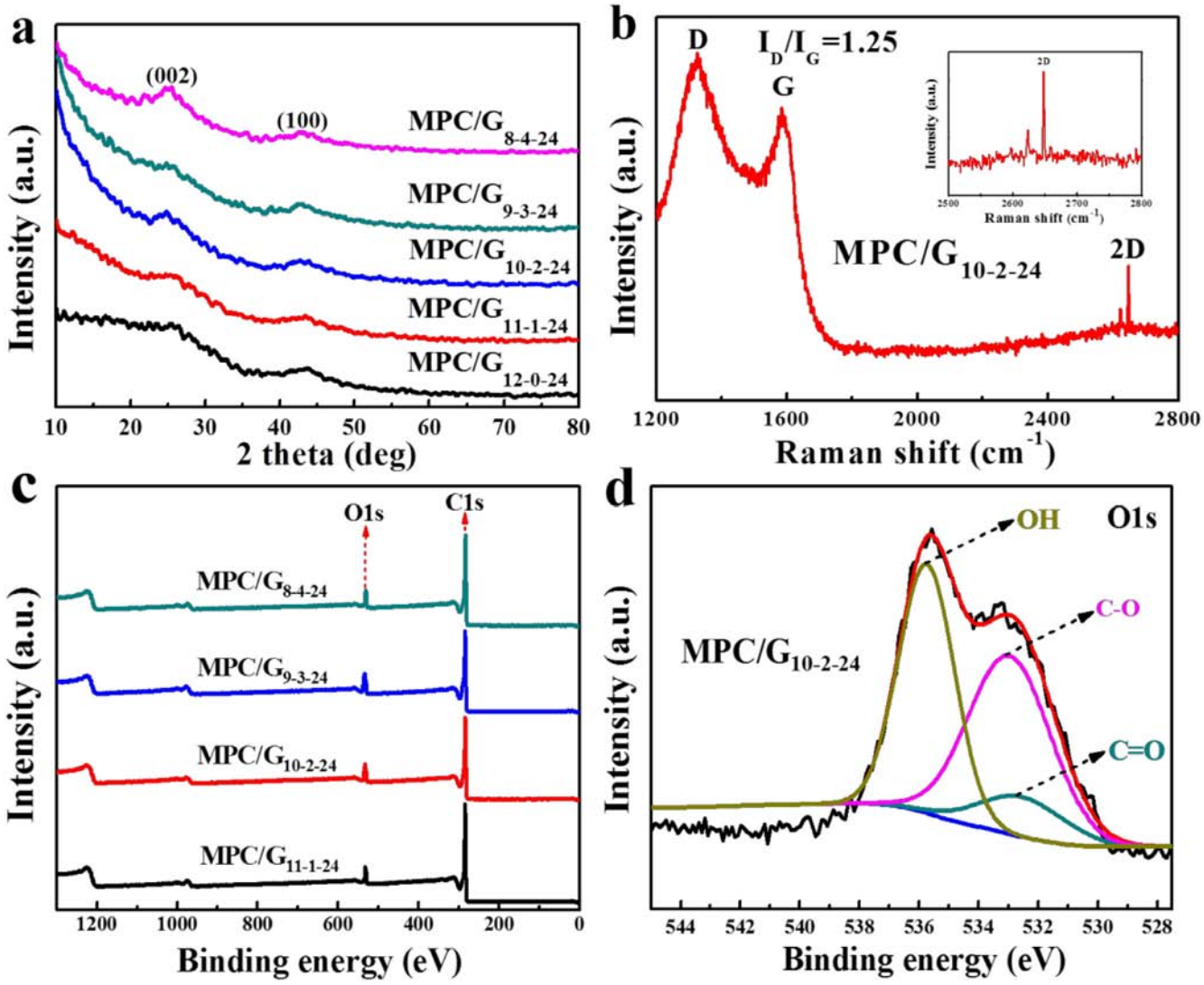

Fig. 3. (a) XRD patterns of MPC/G composites; (b) Raman spectrum of MPC/$G_{10\text{-}2\text{-}24}$ composite, inset is the magnified 2D peak; (c) XPS spectra of MPC/G composites; (d) O1s spectra of MPC/$G_{10\text{-}2\text{-}24}$ composite.

weak 002 diffraction peaks at $2\theta \approx 25°$, which can be partly assigned to the graphene crystallite structure in MPC/G composites. In addition, the 100 diffraction peaks can be observed at $2\theta \approx 43°$, suggesting that the carbon materials possess a few graphitic frameworks due to the reduction of GO into graphene. The Raman spectra in the range of 1200–2800 cm^{-1} was analyzed to further study the structure of MPC/$G_{10\text{-}2\text{-}24}$, and the result are presented in Fig. 3b. It can be clearly seen that the obtained samples exhibit three featured bands, a *D*-band (1327 cm^{-1}) associated with structural defects and partially disordered structures in carbon materials; a G-band (1585 cm^{-1}) related to the E_{2g} vibration mode of 2D graphite; and a 2D-band (2750 cm^{-1}), the characteristic band of graphite carbon materials [26]. The magnified 2D peak is shown as an inset in Fig. 3b, which is ascribed to the existence of graphene in the composites. It was reported that carbon monoxide was formed during the KOH activation [27], which may reduce GO into graphene sheets. The intensity ratio of the D-band to G-band (I_D/I_G) depends on the type of graphitic materials and reflects the crystallinity of these materials. As shown in Fig. 3b, the value of I_D/I_G is 1.25, indicating that MPC/$G_{10\text{-}2\text{-}24}$ belongs to amorphous material. This result is consistent with the above XRD results. Fig. 3c presents the XPS spectra of the MPC/G composites. Only the C1s and O1s peaks are found in the XPS spectra, indicating that no impurities are found in the MPC/G composites. The O1s peaks was deconvoluted into oxygen double bonded to carbon (C═O) (531.9 eV), oxygen single bonded to carbon in C—O (533.4 eV), and oxygen in hydroxyl (OH), as shown in Fig. 3d. The contents of C and O elements in the MPC/G composites are shown in Table 2. The XPS results show that the oxygen-containing groups including C═O, C—O and OH. Some oxygen-containing functional groups are expected to improve the wettability between electrode materials and electrolytes, depending on their hydrophilic nature, and prevent aggregation of adjacent graphene sheets [28].

Table 2
Contents of C and O elements in the MPC/G composites.

MPC/G samples	C1s (%)	O1s (%)	O1s		
			C = O (%)	*C*-O (%)	*O*-H (%)
MPC/$G_{11\text{-}1\text{-}24}$	84	16	6.1	7.1	2.8
MPC/$G_{10\text{-}2\text{-}24}$	79	21	2.3	9.6	9.1
MPC/$G_{9\text{-}3\text{-}24}$	74	26	1.5	8.3	16.2
MPC/$G_{8\text{-}4\text{-}24}$	82	18	7.3	8.4	2.3

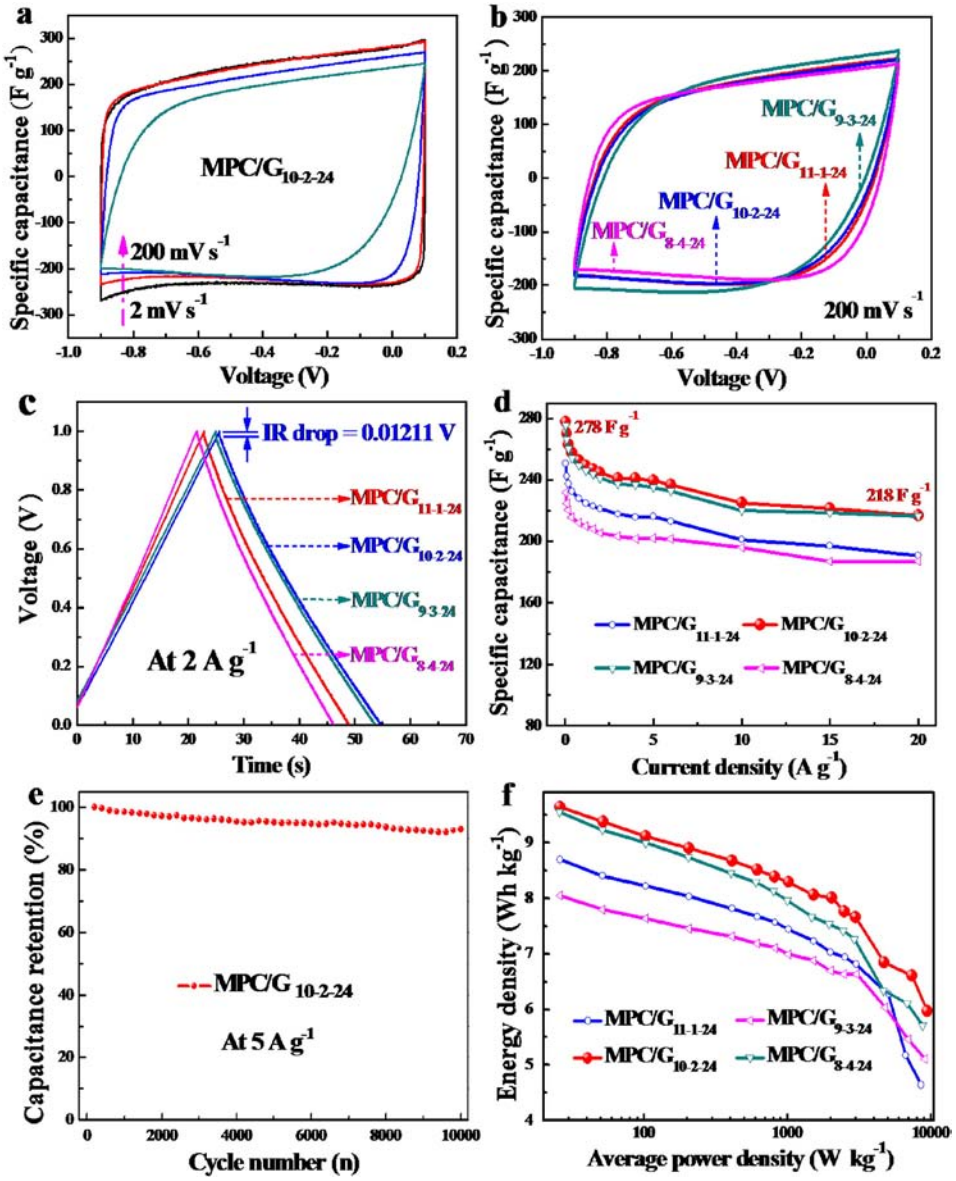

Fig. 4. (a) CV curves of MPC/$G_{10\text{-}2\text{-}24}$ electrode; (b) CV curves of MPC/G electrodes at 200 mV s^{-1} in 6 M KOH aqueous electrolyte; (c) the charge-discharge curves of the MPC/G electrodes; (d) variation of the specific capacitance of the MPC/G electrode with the current densities; (e) capacitance retention of MPC/$G_{10\text{-}2\text{-}24}$ electrode vs. cycle number; (f) Ragone plots of MPC/G capacitors.

3.2. Electrochemical performance of MPC/G composite

Fig. 4a shows the CV curves of MPC/$G_{10\text{-}2\text{-}24}$ composite at scan rates from 2 to 200 mV s^{-1} in 6 M KOH aqueous electrolyte. The symmetric rectangular shape of CV curves is indicative of the typical capacitive behavior, implying quick ion diffusion and good charge propagation to micropores at low scan rate [29]. The symmetric rectangular shape of CV curves indicates the good rate capability of MPC/$G_{10\text{-}2\text{-}24}$ at high discharge current density. The rectangular-shaped CV curves gradually collapse with increasing scan rate owing to diffusion limitation of electrolyte ions at high scan rate. The CV curves of the four MPC/G electrodes at 200 mV s^{-1} are shown in Fig. 4b, indicating the good diffusion rate of ions at high scan rate. For an ideal EDLC, the kinetic process of ion transfer is not limited, and it will be a rectangular-shaped curve of current (or converted specific capacitance) versus potential (or voltage) if the responding current keeps a constant at a certain scan rate in the CV measurements. The rectangular degree of the CV curves reflects the ion diffusion rate within the pores of electrodes. The higher the rectangular degree is, the bigger the ion diffusion rate will be [30].

The gavanostatic charge/discharge test can be used to accurately determine the specific capacitance of electrode materials for surpercapacitors. Fig. 4c presents the typical charge/discharge curves of MPC/G electrodes at a current density of 2 A g^{-1}. Fig. 4d shows the variation of the specific capacitance of MPC/G electrodes vs. the discharge current density in 6 M KOH aqueous electrolyte. It can be found that the specific capacitance decreases slowly with the increase of current density from 0.05 A g^{-1} to 20 A g^{-1}, which is due to diffusion limitation of electrolyte ions at high current density [31]. The MPC/$G_{10\text{-}2\text{-}24}$ electrode shows the biggest specific capacitance (278 F g^{-1} at 0.05 A g^{-1}) among the MPC/G electrodes tested. When the discharge current density is increased to 20 A g^{-1}, the capacitance of the MPC/$G_{10\text{-}2\text{-}24}$ composite remains 218 F g^{-1}, showing high

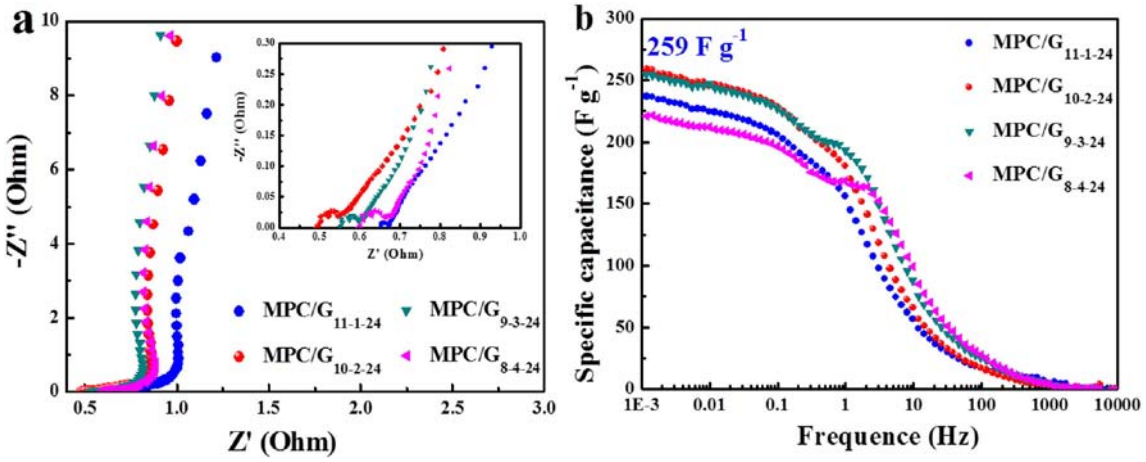

Fig. 5. (a) Nyquist plots of MPC/G composite electrodes; (b) specific capacitance of MPC/G composite electrodes at different frequencies.

capacitance retention up to 78.4% and excellent rate performance. The capacitance of porous carbon reported in our previous work is 171 F g^{-1} in 6 M KOH electrolyte [25]. The excellent performance of MPC/$G_{10\text{-}2\text{-}24}$ composite is ascribed to its high surface area, well-balanced micropores and mesopores for ion fast transport and storage, and dispersed graphene sheets in the composite for good electron conduction. High capacitance and good rate performance of MPC/$G_{10\text{-}2\text{-}24}$ composite are consistent with the results obtained from the CV curves. The capacitance of MPC/$G_{10\text{-}2\text{-}24}$ composite electrode are higher than those reported in literature [23,32]. Fig. 4e shows the variation of the capacitance retention of MPC/$G_{10\text{-}2\text{-}24}$ with the cycle number. The capacitance retention of MPC/$G_{10\text{-}2\text{-}24}$ is up to 93% after 10,000 cycles, indicating good cycle stability. Fig. 4f shows the variation of the energy density of MPC/G capacitors with the average power density. The energy density of MPC/$G_{10\text{-}2\text{-}24}$ capacitor reaches 9.64 Wh kg^{-1} at 0.05 A g^{-1} in 6 M KOH aqueous electrolyte. When the discharge current density is increased to 20 A g^{-1}, the energy density retention of MPC/$G_{10\text{-}2\text{-}24}$ capacitor is as high as 62.5%. Interestingly, the energy density of MPC/$G_{10\text{-}2\text{-}24}$ capacitor in MIMPF_6 electrolyte remains at 43 Wh kg^{-1} at 3665 W kg^{-1}, and 23 Wh kg^{-1} at 5467 W kg^{-1}, which are both bigger that of capacitor fabricated from mesoporous carbon, e.g. 28 Wh kg^{-1} at 1684 W kg^{-1}, and 12 Wh kg^{-1} at 2159 W kg^{-1}, respectively [33].

Fig. 5**a** gives the Nyquist plots of MPC/G composite electrodes. The inset in Fig. 5a is the magnified part of Nyquist plots of MPC/G composite electrodes. The contact resistances of MPC/G composite electrodes between electrode materials and electrolyte only range from 0.5 Ω to 1.65 Ω. At low frequency, the short x-intercept and negligible semicircle of MPC/$G_{10\text{-}2\text{-}24}$ composite electrode reveal that the MPC/$G_{10\text{-}2\text{-}24}$ composite electrode has very low internal resistance, charge-discharge resistance and excellent pore accessibility for the electrolyte ions. At low frequency, the imaginary part sharply increases and nearly vertical lines are observed, suggesting the pure capacitive behavior of the MPC/G composite electrodes [23]. Fig. 5b presents the variations of the specific capacitance with the frequency for the MPC/G electrode. Generally, the larger pores (>2 nm) are easier for electrolyte ions to penetrate at high frequencies, whereas some micropores can only be penetrated at very low frequency. At low frequency (1 mHz), the capacitance of MPC/$G_{10\text{-}2\text{-}24}$ reaches 259 F g^{-1}, which is higher than that of CNTs/AC hybrid [34], meaning that the ionic diffusion to the active surface is more efficient in the case of MPC/$G_{10\text{-}2\text{-}24}$ at higher frequencies due to the excellent architecture of MPC/$G_{10\text{-}2\text{-}24}$.

4. Conclusions

MPC/G composites for high-performance supercapacitors were made directly from CTP and GO by KOH activation. The MPC/G composites possess two advantages, e.g. incorporated graphene for high electron conduction, abundant micropores for ion storage. As the electrodes of supercapacitors, MPC/$G_{10\text{-}2\text{-}24}$ exhibits high specific capacitance (278 F g^{-1} at 0.05 A g^{-1}), good rate performance (remaining at 218 F g^{-1} at 20 A g^{-1}), and excellent cycle stability (with 93% capacitance retention after 10,000 cycles). This work paves a simple method to produce low-cost composite materials. In addition, the method reported here are believed to be of interest for a wide audience of readers in the fields of energy conversion and storage.

Supplementary data to this article can be found online at http://dx.doi.org/10.1016/j.diamond.2016.04.005.

Prime novelty statement

For the first time, microporous carbon/graphene composites (MPC/Gs) with incorporated graphene for high electron conduction and well-developed micropores for abundant ion adsorption were synthesized directly from coal tar pitch and graphene oxide by KOH activation method for supercapacitors. The MPC/G composite electrodes exhibit high specific capacitance, good rate performance and excellent cycle stability. This work paves a facile method to produce composite materials, which is believed to be of interest for a wide audience of readers in the fields of energy conversion and storage.

Acknowledgements

This work was partly supported by the NSFC (Nos. 51272004 and U1361110), the Program for New Century Excellent Talents of the Education Ministry of China (No. NCET-13-0643).

References

[1] J. Gao, X.Y. Wang, Q.L. Zhao, Y.W. Zhang, J. Liu, Synthesis and supercapacitive performance of three-dimensional cubic-ordered mesoporous carbons, Electrochim. Acta 163 (2015) 223–231.
[2] M. Beidaghi, Y. Gogotsi, Capacitive energy storage in micro-scale devices: recent advances in design and fabrication of microsupercapacitors, Energy Environ. Sci. 7 (2014) 867–884.
[3] C.L. Long, X. Chen, L.L. Jiang, L.J. Zhi, Z.J. Fan, Porous layer-stacking carbon derived from in-built template in biomass for high volumetric performance supercapacitors, Nano Energy 12 (2015) 141–151.
[4] Y.Y. Zhang, Z. Zhen, Z.L. Zhang, J.C. Lao, J.Q. Wei, K.L. Wang, F.Y. Kang, H.W. Zhu, In-situ synthesis of carbon nanotube/graphene composite sponge and its application as compressible supercapacitor electrode, Electrochim. Acta 157 (2015) 134–141.
[5] L.X. Fang, B.L. Zhang, W. Li, J.Z. Zhang, K.J. Huang, Q.Y. Zhang, Fabrication of highly dispersed ZnO nanoparticles embedded in graphene nanosheets for high performance supercapacitors, Electrochim. Acta 148 (2014) 164–169.
[6] H.X. Ji, X. Zhao, Z.H. Qiao, J. Jung, Y.W. Zhu, Y.L. Lu, L.L. Zhang, A.H. MacDonald, R.S. Ruoff, Capacitance of carbon-based electrical double-layer capacitors, Nat. Commun. 5 (2014) 3317.

[7] Y.H. Liu, R.T. Wang, J.W. Lang, X.B. Yan, Insight into the formation mechanism of graphene quantum dots and the size effect on their electrochemical behaviors, Phys. Chem. Chem. Phys. 17 (2015) 14028–14035.
[8] J. Yan, T. Wei, B. Shao, F.Q. Ma, Z.J. Fan, M.L. Zhang, C. Zheng, Y.C. Shang, W.Z. Qian, F. Wei, Electrochemical properties of graphene nanosheet/carbon black composites as electrodes for supercapacitors, Carbon 48 (2010) 1731–1737.
[9] X.Y. Chen, C. Chen, Z.J. Zhang, D.H. Xie, High performance porous carbon through hard–soft dual templates for supercapacitor electrodes, J. Mater. Chem. A 1 (2013) 7379–7383.
[10] J.Y. Qu, C. Geng, S.Y. Lv, G.H. Shao, S.Y. Ma, M.B. Wu, Nitrogen, oxygen and phosphorus decorated porous carbons derived from shrimp shells for supercapacitors, Electrochim. Acta 176 (2015) 982–988.
[11] X.L. Yan, X.J. Li, Z.F. Yan, S. Komarneni, Porous carbons prepared by direct carbonization of MOFs for supercapacitors, Appl. Surf. Sci. 308 (2014) 306–310.
[12] Z.J. Li, W. Lv, C. Zhang, B.H. Li, F.Y. Kang, Q.H. Yang, A sheet-like porous carbon for high-rate supercapacitors produced by the carbonization of an eggplant, Carbon 92 (2015) 11–14.
[13] L.L. Jiang, L.Z. Sheng, C.L. Long, Z.J. Fan, Densely packed graphene nanomesh-carbon nanotube hybrid film for ultra-high volumetric performance supercapacitors, Nano Energy 11 (2015) 471–480.
[14] Q.L. Hao, X.F. Xia, W. Lei, W.J. Wang, J.S. Qiu, Facile synthesis of sandwich-like polyaniline/boron-doped graphene nano hybrid for supercapacitors, Carbon 81 (2015) 552–563.
[15] C. Zheng, X.F. Zhou, H.L. Cao, G.H. Wang, Z.P. Liu, Synthesis of porous graphene/activated carbon composite with high packing density and large specific surface area for supercapacitor electrode material, J. Power Sources 258 (2014) 290–296.
[16] R. Raccichini, A. Varzi, S. Passerini, B. Scrosati, The role of graphene for electrochemical energy storage, Nat. Mater. 14 (2015) 271–279.
[17] Z.J. Fan, J. Yan, L.J. Zhi, Q. Zhang, T. Wei, J. Feng, M.L. Zhang, W.Z. Qian, F. Wei, A three-dimensional carbon nanotube/graphene sandwich and its application as electrode in supercapacitors, Adv. Mater. 22 (2010) 3723–3728.
[18] X.J. He, P.H. Ling, J.S. Qiu, M.X. Yu, X.Y. Zhang, M.D. Zheng, Efficient preparation of biomass-based mesoporous carbons for supercapacitors with both high energy density and high power density, J. Power Sources 240 (2013) 109–113.
[19] X.M. Fan, C. Yu, J. Yang, Z. Ling, C. Hu, M.D. Zhang, J.S. Qiu, A layered-nanospace-confinement strategy for the synthesis of two-dimensional porous carbon nanosheets for high-rate performance supercapacitors, Adv. Energy Mater. 5 (2015) 1401761.
[20] Z.P. Chen, C. Xu, C.Q. Ma, W.C. Ren, H.M. Cheng, Lightweight and flexible graphene foam composites for high-performance electromagnetic interference shielding, Adv. Mater. 25 (2013) 1296–1300.
[21] X.L. Wu, L.L. Jiang, C.L. Long, Z.J. Fan, From flour to honeycomb-like carbon foam: carbon makes room for high energy density supercapacitors, Nano Energy 13 (2015) 527–536.
[22] X.J. He, L. Jiang, S.C. Yan, J.W. Lei, M.D. Zheng, H.F. Shui, Direct synthesis of porous carbon nanotubes and its performance as conducting material of supercapacitor electrode, Diam. Relat. Mater. 17 (2008) 993–998.
[23] G.G. Sun, B. Li, J.B. Ran, X.Y. Shen, H. Tong, Three-dimensional hierarchical porous carbon/graphene composites derived from graphene oxide-chitosan hydrogels for high performance supercapacitors, Electrochim. Acta 171 (2015) 13–22.
[24] J. Yan, T. Wei, W.M. Qiao, B. Shao, Q.K. Zhao, L.J. Zhang, Z.J. Fan, Rapid microwave-assisted synthesis of graphene nanosheet/Co_3O_4 composite for supercapacitors, Electrochim. Acta 55 (2010) 6973–6978.
[25] X.J. He, X.J. Li, X.T. Wang, N. Zhao, M.X. Yu, M.B. Wu, Efficient preparation of porous carbons from coal tar pitch for high performance supercapacitors, New Carbon Mater. 29 (2014) 493–502.
[26] Y.F. Song, S. Hu, X.L. Dong, Y.G. Wang, C.X. Wang, Y.Y. Xia, A nitrogen-doped hierarchical mesoporous/microporous carbon for supercapacitors, Electrochim. Acta 146 (2014) 485–494.
[27] X.J. He, N. Zhao, J.S. Qiu, N. Xiao, M.X. Yu, C. Yu, X.Y. Zhang, M.D. Zheng, Synthesis of hierarchical porous carbons for supercapacitors from coal tar pitch with nano-Fe_2O_3 as template and activation agent coupled with KOH activation, J. Mater. Chem. A 1 (2013) 9440–9448.
[28] Z.Y. Lin, Y. Liu, Y.G. Yao, O.J. Hildreth, Z. Li, K. Moon, C.P. Wong, Superior capacitance of functionalized graphene, J. Phys. Chem. C 115 (2011) 7120–7125.
[29] M.B. Wu, P.P. Ai, M.H. Tan, B. Jiang, Y.P. Li, J.T. Zheng, W.T. Wu, Z.T. Li, Q.H. Zhang, X.J. He, Synthesis of starch-derived mesoporous carbon for electric double layer capacitor, Chem. Eng. J. 245 (2014) 166–172.
[30] X.J. He, H.B. Zhang, H. Zhang, X.J. Li, N. Xiao, J.S. Qiu, Direct synthesis of 3D hollow porous graphene balls from coal tar pitch for high performance supercapacitors, J. Mater. Chem. A 2 (2014) 19633–19640.
[31] M. Ramezani, M. Fathi, F. Mahboubi, Facile synthesis of ternary MnO_2/graphene nanosheets/carbon nanotubes composites with high rate capability for supercapacitor applications, Electrochim. Acta 174 (2015) 345–355.
[32] Q.H. Liang, L. Ye, Q. Xu, Z.H. Huang, F.Y. Kang, Q.H. Yang, Graphitic carbon nitride nanosheet-assisted preparation of N-enriched mesoporous carbon nanofibers with improved capacitive performance, Carbon 94 (2015) 342–348.
[33] X.J. He, H.B. Zhang, K. Xie, Y.Y. Xia, Z.G. Zhao, X.T. Wang, Synthesis of mesoporous carbons from rice husk for supercapacitors with high energy density in ionic liquid electrolytes, J. Nanosci. Nanotechnol. 16 (2016) 2841–2846.
[34] X. Geng, L.X. Li, F. Li, Carbon nanotubes/activated carbon hybrid with ultrahigh surface area for electrochemical capacitors, Electrochim. Acta 168 (2015) 25–31.